Truss Topology Optimization of Steel-Timber Structures for Embodied Carbon Objectives

by

Ho Yin Ernest Ching

B.S. Civil Engineering
University of California, Los Angeles, 2019

Submitted to the Department of Civil and Environmental Engineering
in Partial Fulfillment of the Requirements for the Degree of

MASTER OF ENGINEERING IN CIVIL AND ENVIRONMENTAL ENGINEERING

AT THE

MASSACHUSETTS INSTITUTE OF TECHNOLOGY

MAY 2020

Signature of Author: _____
Department of Civil and Environmental Engineering
May 8, 2020

Certified by: _____
Josephine V. Carstensen
Assistant Professor of Civil and Environmental Engineering
Thesis Supervisor

Accepted by: _____
Colette L. Heald
Professor of Civil and Environmental Engineering
Chair, Graduate Program Committee

This page is left blank intentionally.

Truss Topology Optimization of Steel-Timber Structures for Embodied Carbon Objectives

by

Ho Yin Ernest Ching

Submitted to the Department of Civil and Environmental Engineering on May 8th 2020 in Partial Fulfilment of the Requirements for the Degree of Master of Engineering in Civil and Environmental Engineering

Abstract

Topology optimization in structural design is still a relatively new tool. Most existing research on truss and frame structures focuses on single material applications, and the developments of ground structure-based topology optimization in multi-material structures are limited. This research presents a truss topology optimization algorithm that designs with a mix of glue-laminated timber (GLT) and steel elements. The motivation behind allowing the choice of both these materials is to utilize the strengths of each material in both tension and compression. In addition, this work seeks to include environmental consideration, by incorporating in the algorithm that timber has a smaller embodied carbon coefficient (ECC) compared to steel.

This work uses the ground structure approach to truss topology optimization and designs are generated and compared using (i) a minimum compliance and (ii) a stress-constrained algorithm. The algorithms are constructed such that both the area and a choice of material is made for each element in the ground structure. Both frameworks use fmincon in MATLAB as the gradient-based optimizer. The Solid Isotropic Material with Penalization (SIMP) interpolation is used to relate elastic modulus and embodied carbon for two materials with respect to normalized density variables. To demonstrate the versatility of this design methodology, designs obtained from different objectives and different constraints are presented and compared.

We find that, for minimum compliance objectives, the weight-constrained problem produced all-steel truss solutions, while global warming potential (GWP)-constrained problem produced all-timber truss solutions. These results align with our expectations based on material stiffness properties. For the stress-constrained problem with minimum GWP objectives, the solutions obtained from two modeling assumptions were compared: (i) with real material stress constraints and (ii) with modified stress constraints, where timber was considered as a compression-only material and steel as a tension-only material. Surprisingly, we find that the solutions obtained with the real stress limits are more polluting than the modified stress limit solutions. While the modified stress solutions placed steel in tension and timber in compression for the most environmentally friendly design, the real stress solutions generally favored steel over timber. This is believed to be caused by the nonlinearities introduced through the SIMP interpolation.

Keywords: Topology Optimization, Multi-Material, Truss, Embodied Carbon

Thesis Supervisor: Josephine V. Carstensen
Title: Assistant Professor of Civil and Environmental Engineering

This page is left blank intentionally.

Acknowledgements

I would like to express my deepest gratitude to my thesis and academic adviser, Professor Josephine V, Carstensen, for her mentorship and encouragement. Without her guidance and help, the goal of this thesis would not have been realized. Professor Carstensen, thank you for believing in me when I needed it most.

I am eternally grateful to my family for their unconditional support throughout my education. I could not have done it without you.

This page is left blank intentionally.

Table of Contents

1. Introduction

The building and construction industry is a major source of global carbon emissions, due to a combination of operational carbon and embodied carbon. Operational carbon is proportional to operational energy, which is the energy used to light, heat, cool, ventilate, and operate the functions of the building. Embodied carbon accounts for carbon emissions due to "material extraction, transport to sites, construction, maintenance, and demolition" [1].

In 2018, residential and commercial buildings accounted for a total of 39% of U.S. energy consumptions, as shown in Figure 1.1 [2]. Operational carbon generally constitutes a larger fraction of building carbon footprints than embodied carbon (75% in a new-building housing case study [3]). Until recently, most research related to reducing building carbon footprints has focused on operational carbon and energy. As operational carbon is reduced through various energy efficient measures, the impact of embodied carbon becomes greater.

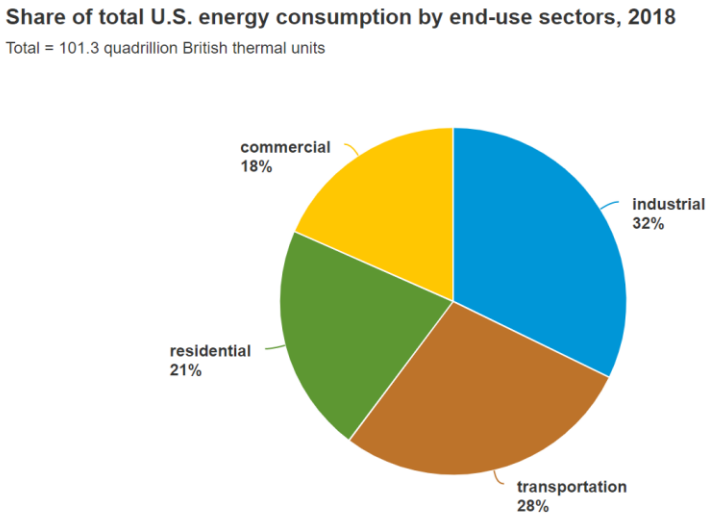

Figure 1.1: Share of total U.S. energy consumption by end-use sectors, 2018 [2]

In a case study of 78 office buildings, it was found that embodied carbon attributed to structural elements (steel, concrete, plaster and brick) accounted for 60% of total embodied carbon [4]. Hence, reducing structural embodied carbon can have a large impact on reducing the total embodied carbon of a building. Several studies have proposed tools to measure and benchmark the embodied carbon content of buildings [5]–[8]. A 2016 study highlights several mitigation strategies to lower building embodied carbon, including the selection of low embodied carbon materials, and better design practices [9]. However, since interest into reducing structural embodied carbon is still relatively new, there has been a lack of design methods for

the goal of reducing the structural embodied carbon footprint [10]. One proposed method is to use sizing and shape optimization for the goal of minimizing global warming potential (GWP), as presented in a 2018 MIT thesis [11].

This paper presents a new design method, utilizing multi-material truss topology optimization for minimum GWP objectives. Topology optimization is a generalized type of sizing optimization, where optimized member sizes and connectivity are found through an iterative algorithm [12] (refer to Section 3 for more details). While topology optimization has been used extensively in mechanical and aerospace applications, its use in structural design is still a relatively new tool [13]. Most existing research on truss topology optimization focuses on single material applications, and the study on topology optimization in multi-material structures is limited.

We are interested in multi-material structures in order to employ different materials for their respective strengths. Since different materials can have relative strengths and weaknesses depending on loading direction (e.g. tension, compression, bending, and twisting), utilizing each material in its strongest loading direction produces the most structurally efficient design. For example, generally speaking, steel performs better in tension while timber performs better in compression [11]. Steel is more susceptible to compression buckling due to its slenderness, and timber is 30% weaker in tension due to non-uniformity in wood grain orientation [14]. Moreover, timber is a more environmentally friendly material, with an embodied carbon content (per unit weight) 3.5 times smaller than that of steel [15]. Example built examples of timber-steel trusses are shown in Figure 1.2 [16] & Figure 1.3 [17].

To demonstrate the potential of the proposed design methodology, this thesis studies the topology optimization of 2D and 3D truss structures, constructed with a mix of glue-laminated timber (GLT) and steel elements.

Figure 1.2: Timber-steel roof at the Scottish Parliament (Photograph: Wikimedia Commons – Mogens Engelund)

Figure 2.3: Timber-steel roof at UMass Amherst Design Building (Photograph: Albert Vecerka)

2. Literature Review

This section first reviews previous research on benchmarking material embodied carbon contents and design methods for embodied carbon objectives. Then, previous research on truss topology optimization involving multiple materials is also reviewed. The final subsection discusses how this thesis will expand upon these previous works by proposing a new design methodology involving multi-material truss topology optimization.

2.1 Benchmarking Embodied Carbon & Existing Design Methods for Embodied Carbon Objectives

In recent years, there has been a growing interest in measuring and benchmarking the embodied carbon content of different materials and building types [5]–[8], due to the increasing impact of building embodied carbon on the total building carbon footprint and climate change. Since material embodied carbon coefficients (the ratio of mass of CO2 produced over unit mass of material) vary depends on multiple factors including region, sourcing choice, building lifespan, and end-of-life treatment [1], there can be different numbers for the embodied carbon coefficient for the same material. To select an appropriate and consistent measure for the embodied carbon coefficients of steel and timber, the values from University of Bath's Inventory of Carbon and Energy database [15] are used in this study, which were calculated based on averages and specified assumptions. The material properties of 50 ksi steel [18] and Douglas Fir Grade L3 glue-laminated timber (GLT) [14], with their respective embodied carbon coefficients, are presented and compared in Table 2.1.

As revealed by the numbers in Table 2.1, per unit volume, steel is 18 times stiffer than timber, but only 14 times heavier. In other words, **steel is 1.3 times stiffer per unit weight than timber.** On the other hand, (per unit volume,) steel is 18 times stiffer than timber, but 47 times more polluting. This means that **timber is 2.6 times stiffer per unit mass of embodied carbon compared to steel, making timber the "greener" choice for stiffness considerations.**

For strength considerations, per unit volume, steel is 53 times and 40 times stronger in tension and compression respectively (compared to timber), and 47 times more polluting. This implies **steel is 1.13 times stronger (than timber) in tension per unit mass of embodied carbon, but timber is 1.18 times stronger (than steel) in compression per unit mass of embodied carbon. Therefore, the best choice of material depends on design objectives as well as loading conditions.**

Table 2.1: Comparison of material properties of steel and glue-laminated timber (GLT)

Material Property	**Symbol**	**Steel** [18]	**Timber (GLT)** [14]	**Per unit volume, steel is:**
Elastic Modulus (ksi)	***E***	29000	1600	**18 times stiffer**
Yield Stress (psi)	σ_y	50000	-1250 / +950	**-40 / +53 times stronger**
Density (pcf)	ρ	491	35.6	**14 times heavier**
Embodied Carbon Coefficient, ($lb_{CO2}/lb_{material}$) [15]	***ECC***	1.46	0.42	**47 times more polluting**

Note: where specified, "-" denotes compression and "+" denotes tension.

Regarding design methods for embodied carbon objectives, most existing research have focused on current design practices for embodied carbon at the building scale [9], [10]. To the best of the author's knowledge, the only existing research on reducing embodied carbon using structural optimization is a 2018 MIT thesis by Stern [11]. The 2018 thesis used shape and sizing optimization to study planar truss structures of various spans and compared the global warming potentials (GWP) of single-material and steel-timber designs. Her thesis found that compared to a baseline all-steel truss, a steel-timber truss with shape and sizing optimization yields savings of 31% - 57% depending on span length. Stern's research is important because it was the first comprehensive study on the combination of structural optimization, embodied carbon, and sustainability comparisons between materials; most existing works on structural optimization focused on weight minimization, which Stern found does not necessarily correlate to global warming potential (GWP) minimization.

2.2 Existing Research on Truss Topology Optimization

Although there is an abundance of existing research on the design of multi-material continuum topology optimization [19]–[22], there has been relatively few for multi-material truss topology optimization.

Most existing literature of truss topology optimization focuses on single-material examples. Truss topology optimization has mainly been focused on designing for compliance or weight subject to stress and local buckling constraints [23]–[26]. Extensions of these works have also addressed global buckling considerations [27], [28]. In the context of truss topology optimization for civil scale structures, most works have focused on the automatic generation of strut-and-tie layouts for reinforced concrete (RC) design [29], [30], incorporating imperfections and uncertainties [31], [32] and implementing a cost for manufacturability [33].

Several pieces of literature involving multi-material truss topology optimization are reviewed here. In 1996, a paper by Achtziger studied truss topology optimization including different bar properties for tension and compression for a single material [34]. Comparing the resulting structures of the studied trusses, Achtziger concluded that "different treatment of bars being under tension or under compression heavily influences the optimal design obtained." This is significant because it showed that, for a given material with different tensile and compressive strengths, the final topology changes depending on the pair of strengths provided to the optimizer.

The next piece of literature by Stolpe and Svanberg (2004) investigated the problem of simultaneously selecting the material and determining the area of each bar in a truss to minimize the cost of the structure, subject to stress constraints under a single load condition [35]. By examining the mathematical optimization problem, they showed that two different materials are always sufficient in an optimal truss. In the case that one material has a higher allowable stress in both compression and tension (compared to other materials considered), one material is sufficient. This conclusion may seem obvious, but note that it does not hold if there are several loading conditions.

Lastly, a 2008 paper by Rakshit and Ananthasuresh explored simultaneous geometry design and material selection of statically determinate trusses [36]. The 2008 study selected the optimal material for truss members from an material database, but only allowed single-material trusses for the final design. Instead of starting from a densely meshed and connected ground structure (as in general truss topology optimization), they assumed a simpler geometry for the truss, and took the geometry variables (member areas, lengths & orientations) as design variables.

2.3 Problem Statement

While existing research has benchmarked the embodied carbon of materials, reviewed current design practices for embodied carbon objectives on a building scale, and multi-material truss topology optimization (to a limited degree), to the best of the author's knowledge, there has been no published work on multi-material truss topology optimization for embodied carbon objectives.

Therefore, this thesis aims to bridge the knowledge gap between existing literature reviewed in Sections 2.1 & 2.2, by presenting a new design method, utilizing multi-material truss topology optimization for minimum global warming potential (GWP) objectives. This method directly incorporates Pomponi and Mancaster's suggested mitigation strategies on reducing embodied carbon [9] by (i) allowing the choice to use a more environmentally friendly material, timber, in additional to the more commonly used truss material, steel, and by (ii) finding an optimized truss design through topology optimization. From Stolpe and Svanberg [35], we know that two materials (e.g. timber & steel) are sufficient for a truss topology optimization problem with a single load case. This thesis builds on Stern's thesis [11], which performed sizing and shape optimization on planar trusses for GWP objectives, by extending it to topology optimization on both 2D and 3D trusses.

To demonstrate the potential of the proposed design methodology, this thesis studies the topology optimization of truss structures, constructed with a mix of glue-laminated timber (GLT) and steel elements. Section 3 introduces the reader to an overview of single-material truss topology optimization. Section 4 explores the multi-material minimum compliance problem subject to either a weight or a GWP constraint, and Section 5 explores the multi-material stress-constrained problem for a minimum GWP objective.

3. Overview of Single-Material Truss Topology Optimization

This section gives a brief introduction to truss topology optimization and the ground structure approach. A truss is a structure where each and every connection between members are pins that transfer no moments, and where loads are only applied at the nodes [37]. As a result, truss members only carry loads axially, in tension or compression. Truss topology optimization with the ground structure approach is a design problem where an optimized truss topology is found through iteratively solving a generalized sizing optimization problem [12], as explained below.

To perform topology optimization on a truss structure, the design domain must first be defined. The domain is meshed with nodes (joints where members start and end), boundary conditions are defined, and loads are applied at the desired nodes.

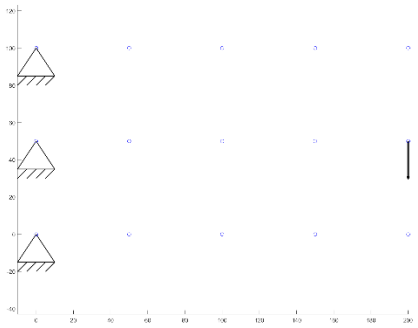

Figure 3.1: Design domain with nodes, boundary conditions, and loading

Element connectivity of the ground structure is then defined. For example, a ground structure can be fully connected (Figure 3.2(a)) or X-braced (Figure 3.3(a)).

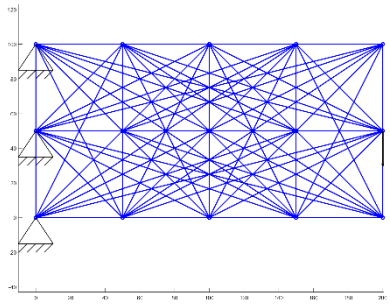

Figure 3.2(a): Fully connected, ground structure

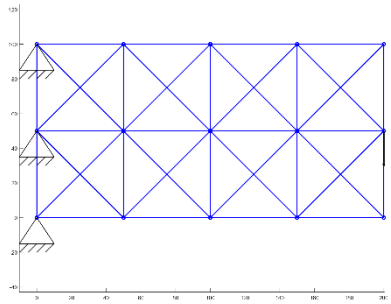

Figure 3.3(a): X-braced, ground structure

Sizing optimization is performed. A common optimization objective used in topology (and sizing) optimization is minimum compliance, due to ease and speed of computation. Minimizing compliance (force multiplied by displacement) is equivalent to maximizing the elastic stiffness of the structure.

(Eq. 3.1) – Problem formulation for a min compliance problem subject to a weight constraint:

$$
\begin{aligned}
&\underset{A^e}{minimize} && F^T u && \leftarrow \text{Compliance} \\
&subject\ to && K(A^e)u = F && \leftarrow \text{Static Equilibrium} \\
& && \textstyle\sum_{e\in\Omega} A^e L^e \rho^e \ \leq\ W && \leftarrow \text{Weight Constraint} \\
& && A_{min} \leq A^e \ \leq A_{max} \ \ \forall\ e \in \Omega && \leftarrow \text{Bounds on } A^e
\end{aligned}
$$

where:

F^T is the global force vector

u is the global displacement vector

K is the global stiffness matrix

A^e is the truss member area

L^e is the truss member length

ρ^e is the truss member density

W is the specified weight constraint

In Eq. 3.1, the objective function to be minimized is the compliance, with member areas A^e as the design variables. A^e is bounded by A_{min} and A_{max}. The problem is subject to a weight constraint and must satisfy static equilibrium.

Sensitivity Analysis:

In order to solve the design problem, a gradient-based optimizer is used. Gradient-based optimizers require sensitivity information of the objective and constraints as an input. Out of the three general approaches used to compute the sensitivities for structural optimization problems, namely finite difference, direct differentiation, and the adjoint method [38], the adjoint method is used here due to its speed in solving min compliance problems.

In the adjoint method, the equilibrium constraint $\lambda^T(Ku - F) = 0$ can be added to the objective without changing it, since it equals zero. λ is any arbitrary but real fixed vector.

The objective is now:

$$\tilde{f} = F^T u + \lambda^T (Ku - F) \qquad \text{(Eq. 3.2)}$$

And the sensitivity for the objective with respect to design variable A^e is then:

$$\frac{\partial \tilde{f}}{\partial A^e} = F^T \frac{\partial u}{\partial A^e} + \lambda^T \left(\frac{\partial K}{\partial A^e} u + K \frac{\partial u}{\partial A^e}\right) \qquad \text{(Eq. 3.3)}$$

Rearranging, we get:

$$\frac{\partial \tilde{f}}{\partial A^e} = (F^T + \lambda^T K) \frac{\partial u}{\partial A^e} + \lambda^T \frac{\partial K}{\partial A^e} u \qquad \text{(Eq. 3.4)}$$

Defining the adjoint problem as the equilibrium constraint:

$$F^T + \lambda^T K = 0, \qquad \lambda = -u \qquad \text{(Eq. 3.5)}$$

And the sensitivity becomes:

$$\frac{\partial \tilde{f}}{\partial A^e} = -u^T \frac{\partial K}{\partial A^e} u \qquad \text{(Eq. 3.6)}$$

Defining $K^e{}_0$ as follows:

$$K_0^e = \frac{K^e}{A^e E^e} \qquad \text{(Eq. 3.7)}$$

The partial derivative of K with respect to A^e is:

$$\frac{\partial K}{\partial A^e} = E^e K_0^e \qquad \text{(Eq. 3.8)}$$

As we can see here, the adjoint method for min compliance problems is computationally inexpensive since it requires no additional solve, as the displacement vector u is already computed in the equilibrium constraint, and $\frac{\partial K}{\partial A^e}$ is a constant that does not change throughout the iterations. For more details regarding sensitivities, refer to Christensen and Klarbring [38].

The sensitivity for the weight constraint is simply:

$$\frac{\partial g}{\partial A^e} = L^e \rho^e \qquad \text{(Eq. 3.9)}$$

Solving the topology optimization problem:

In each sizing optimization iteration, static equilibrium is satisfied. When subject to a limiting amount of material (or a weight constraint), the gradient-based optimizer uses the supplied sensitivities to determine which members are useful, and which are not (carrying zero forces). Through the iterations, the zero force members become reduced in size, down to A_{min}, the lower bound on A^e. A_{min} is chosen to be a positive number that is very close to 0, e.g. 1e-3. The remaining members become larger in size; members are sized so that a uniform stress distribution across all members is achieved. See Figures 3.2 and 3.3 for visuals on changes in member areas through iterations. When the first order optimality falls within a predetermined tolerance, the design problem has reached convergence and the optimizer terminates.

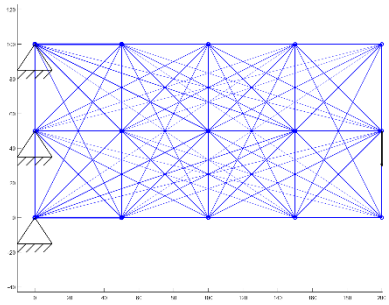

Figure 3.2(b): Fully connected, iteration 1

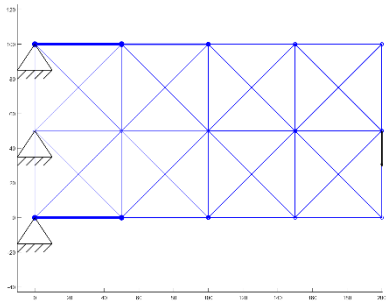

Figure 3.3(b): X-braced, iteration 1

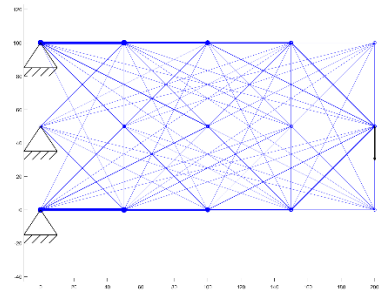

Figure 3.2(c): Fully connected, iteration 5

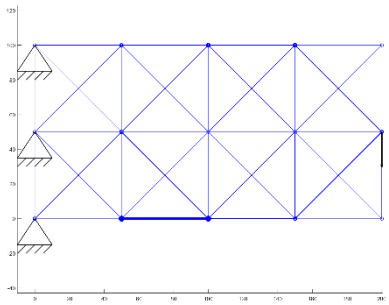

Figure 3.3(c): X-braced, iteration 5

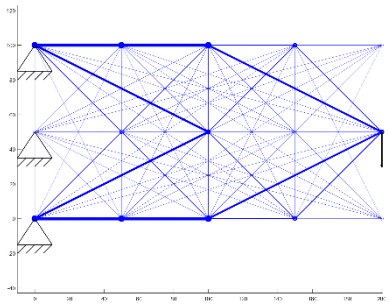

Figure 3.2(d): Fully connected, converged

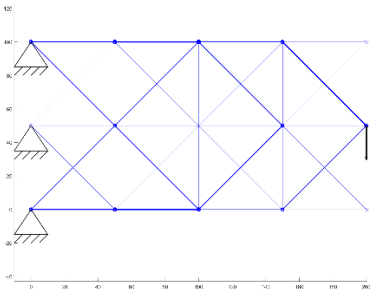

Figure 3.3(d): X-braced, converged

To obtain a cleaner design, members that are very small are removed from the plot. As a result, only members that are useful in resisting the applied load remains (Figure 3.2(e) and 3.3(e)). It can be seen that the fully connected ground structure produces a more free-form solution, while the X-braced ground structure produces a solution that is limited by a combination of vertical, horizontal and 45° diagonal elements.

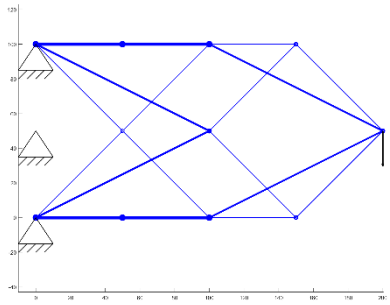

Figure 3.2(e): Fully connected, optimized topology

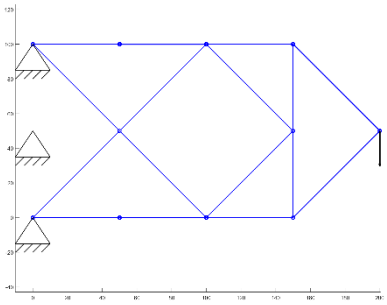

Figure 3.3(e): X-braced, optimized topology

Building upon this framework, the topology optimization problem of multi-material trusses is investigated in this thesis. MATLAB is used as the coding program, with fmincon as the gradient-based optimizer. The min compliance problem of multi-material trusses, subject to a weight or global warming potential (GWP) constraint is discussed in Section 4, and the stress constrained problem with a minimum GWP objective is discussed in Section 5.

4. Multi-Material Truss: Minimum Compliance Problem

4.1 Problem Formulation

The first part of this project investigates multi-material minimum compliance (maximum stiffness) problems subject to either (4.1a) a structural weight constraint or (4.1b) a global warming potential (GWP) constraint.

(Eq. 4.1a) – Minimum compliance subject to weight constraint:

$$
\begin{aligned}
&\underset{A^e, x^e}{minimize} && F^T u && \leftarrow \text{Compliance} \\
&subject\ to && K(A,x)u = F && \leftarrow \text{Static Equilibrium} \\
& && \textstyle\sum_{e\in\Omega} A^e L^e \rho^e \ \leq\ W && \leftarrow \text{Weight Constraint} \\
& && A_{min} \leq A^e \leq A_{max} \quad \forall\ e \in \Omega && \leftarrow \text{Bounds on } A^e \\
& && 0 \leq x^e \leq 1 \quad \forall\ e \in \Omega && \leftarrow \text{Bounds on } x^e
\end{aligned}
$$

(Eq. 4.1b) – Minimum compliance subject to GWP constraint:

$$
\begin{aligned}
&\underset{A^e, x^e}{minimize} && F^T u && \leftarrow \text{Compliance} \\
&subject\ to && K(A,x)u = F && \leftarrow \text{Static Equilibrium} \\
& && \textstyle\sum_{e\in\Omega} A^e L^e (\rho^e ECC^e) \ \leq\ GWP && \leftarrow \text{GWP Constraint} \\
& && A_{min} \leq A^e \leq A_{max} \quad \forall\ e \in \Omega && \leftarrow \text{Bounds on } A^e \\
& && 0 \leq x^e \leq 1 \quad \forall\ e \in \Omega && \leftarrow \text{Bounds on } x^e
\end{aligned}
$$

where:

F, u, K, Ae, Le, ρ^e are as defined in Eq. 3.1

ECC^e is the material embodied carbon coefficient of the truss member

GWP is the specified global warming potential constraint

x^e is the material mapping variable

Since continuous variables are needed for gradient based optimizers (e.g. fmincon in MATLAB), we need to formulate the problem in a way that makes the discrete stiffness variable E^e continuous. We can do that by introducing a new continuous variable, $0 \leq x^e \leq 1$, that relates to E^e and ρ^e (Eqs. 4.2 and 4.3) using Solid Isotropic Material with Penalization (SIMP) interpolation [39]. SIMP is traditionally used in continuum topology optimization to interpolate between voids and fully filled spaces [40]. Here, SIMP is used to

interpolate between the two material stiffnesses (and densities). Hence, we define x^e as the material mapping variable.

$$E^e = (x^e)^\eta \Delta E + E_{timber}\,, \qquad \Delta E = E_{steel} - E_{timber} \qquad \text{(Eq. 4.2)}$$

$$\rho^e = (x^e)^\eta \Delta\rho + \rho_{timber}\,, \qquad \Delta\rho = \rho_{steel} - \rho_{timber} \qquad \text{(Eq. 4.3a)}$$

$$(\rho^e ECC^e) = (x^e)^\eta \Delta(\rho ECC) + \rho_{timber} ECC_{timber},$$
$$\Delta(\rho ECC) = \rho_{steel} ECC_{steel} - \rho_{timber} ECC_{timber} \qquad \text{(Eq. 4.3b)}$$

In SIMP, the exponent term η (see Figure 2.1) penalizes intermediate stiffnesses and densities, encouraging the optimizer to converge to either E_{timber} or E_{steel}: if $x^e = 0$, then Eq. 4.2 yields $E^e = E_{timber}$; if $x^e = 1$, then $E^e = E_{steel}$. Through trial and error, it was determined that η = 3 works well for this problem. For example, for the 5x3 cantilever shown in Figure 4.2, η = 1, 3, 10 all yielded identical final objectives. However, η = 1 took 371 iterations; η = 10 took 334 iterations; but η = 3 only took 129 iterations. This shows that an η that is 1 works, but takes longer because there is no stiffness penalty for intermediate materials. η = 10 also works, but takes longer because the problem becomes very non-linear and difficult to solve. η = 3 is the "sweet spot" that introduces a moderate stiffness penalty for intermediate materials, without making the problem too non-linear.

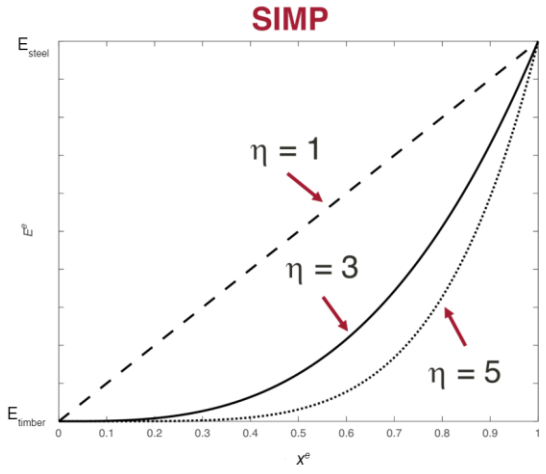

Figure 4.1: SIMP interpolation from x^e to E^e

4.2 Sensitivity Analysis

The sensitivity with respect to design variable A^e for a min compliance problem has been discussed in Section 3 (see Eq. 3.6). Here, we derive the sensitivity with respect to design variable x^e:

With the adjoint method, the objective is now:

$$\tilde{f} = F^T u + \lambda^T (Ku - F) \qquad \text{(Eq. 4.4)}$$

And the sensitivity for the objective with respect to design variable x^e is then:

$$\frac{\partial \tilde{f}}{\partial x^e} = F^T \frac{\partial u}{\partial x^e} + \lambda^T (\frac{\partial K}{\partial x^e} u + K \frac{\partial u}{\partial x^e}) \qquad \text{(Eq. 4.5)}$$

Rearranging, we get:

$$\frac{\partial \tilde{f}}{\partial x^e} = (F^T + \lambda^T K) \frac{\partial u}{\partial x^e} + \lambda^T \frac{\partial K}{\partial x^e} u \qquad \text{(Eq. 4.6)}$$

Defining the adjoint problem as the equilibrium constraint:

$$F^T + \lambda^T K = 0, \qquad \lambda = -u \qquad \text{(Eq. 3.5)}$$

And the sensitivity becomes:

$$\frac{\partial \tilde{f}}{\partial x^e} = -u^T \frac{\partial K}{\partial x^e} u \qquad \text{(Eq. 4.7)}$$

Since

$$E^e = (x^e)^\eta \Delta E + E_{timber}\ , \qquad \text{(Eq. 4.2)}$$

And defining K^e_0 as follows:

$$K_0^e = \frac{K^e}{A^e E^e} \qquad \text{(Eq. 3.7)}$$

The partial derivatives of K with respect to A^e and x^e are:

$$\frac{\partial K}{\partial A^e} = E^e K_0^e \qquad \text{(Eq. 3.8)}$$

$$\frac{\partial K}{\partial x^e} = \frac{\partial K}{\partial E^e} \frac{dE^e}{dx^e} = A^e K_0^e [\eta (x^e)^{\eta - 1} \Delta E] \qquad \text{(Eq. 4.8)}$$

Substituting Eq. 3.8 & Eq. 4.8 into Eq. 3.6 & Eq. 4.7 respectively, we arrive at the full expressions for the sensitivities with respect to A^e and x^e. Note that even with an additional design variable (x^e), the adjoint

method for min compliance remains computationally inexpensive, since u is still computed in the equilibrium, and K^e_0 is a constant throughout the iterations.

The sensitivities for the weight constraint are:

$$\frac{\partial g(weight)}{\partial A^e} = L^e \rho^e \qquad \text{(Eq. 3.9)}$$

$$\frac{\partial g(weight)}{\partial x^e} = A^e L^e [\eta (x^e)^{\eta - 1} \Delta \rho] \qquad \text{(Eq. 4.9)}$$

Similarly, sensitivities for the GWP constraint are:

$$\frac{\partial g(GWP)}{\partial A^e} = L^e (\rho^e ECC^e) \qquad \text{(Eq. 4.10)}$$

$$\frac{\partial g(GWP)}{\partial x^e} = A^e L^e [\eta (x^e)^{\eta - 1} \Delta (\rho ECC)] \qquad \text{(Eq. 4.11)}$$

4.3 Results & Discussion

Cantilevers (Figures 4.2, 4.3 & 4.6), simple beams (Figures 4.4, 4.5 & 4.8) and a vault (Figure 4.7) of different mesh densities in 2D and 3D were topology optimized, subject to (4.1a) a weight constraint or (4.1b) a GWP constraint. Starting with fully connected ground structures, fmincon with the interior-point algorithm was called to perform the optimization. Initial conditions were A_0 = 1 in^2 and x_0 = 0.5 (hypothetical intermediate material), with A^e bound between 1e-3 and 10, and x^e bound between 0 and 1.

The dimensions of each studied structure are shown in Table 4.1. For all structures except the 3D vault, the magnitude of the applied load is 1000 lb, the weight constraint is 1e6 $lbs_{material}$, and the GWP constraint is 1e5 lb_{CO2}. For the 3D vault, the applied load is 2000 lb, the weight constraint is 2.4e5 $lbs_{material}$, and the GWP constraint is 2.4e4 lb_{CO2}.

Table 4.1: Dimensions of each structure

Structure	Height (in)	Length (in)	Depth (in)
2D cantilever (Figs. 4.2 & 4.3)	100	200	N/A
2D simple beam (Figs. 4.4 & 4.5)	100	500	N/A
3D cantilever (Fig. 4.6)	100	200	100
3D vault (Fig. 4.7)	100	100	100
3D simple beam (Fig. 4.8)	100	500	100

The topologies of the ground structure, weight constrained solution, and GWP constrained solution for each examined structure are reported in Tables 4.2 & 4.3. In Table 4.2, the same types of structures modeled with different mesh densities (cantilever: 5x3 vs. 9x5, simple beam: 7x3 vs. 13x5) are compared, revealing that denser meshes yield more complex and free-form solutions, leading to lower compliance objectives.

Table 4.2: Ground structures and optimized solutions for minimum compliance problems (4.1a) & (4.1b), 2D

Ground Structure	(4.1a) Weight Constraint	(4.1b) GWP Constraint
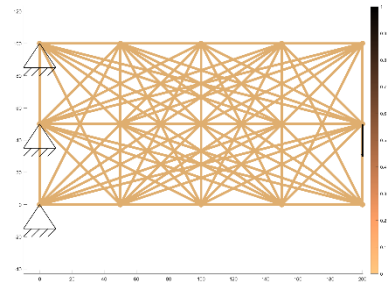	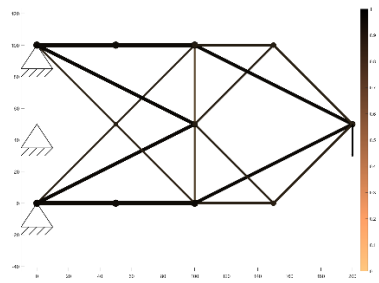	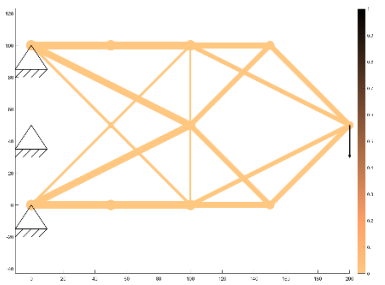
Figure 4.2(a): 5x3 mesh ground structure, cantilever	*Figure 4.2(b): Final structure with weight constraint, cantilever* **Compliance: 9.58**	*Figure 4.2(c): Final structure with GWP constraint, cantilever* **Compliance: 52.6**
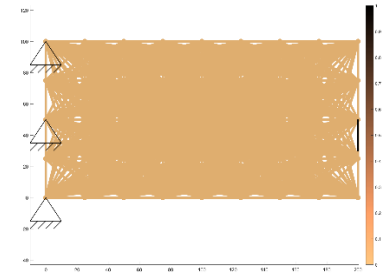	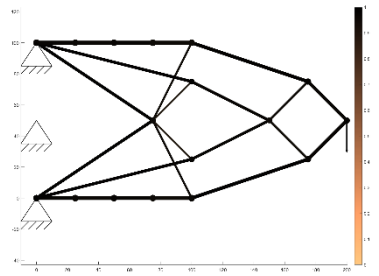	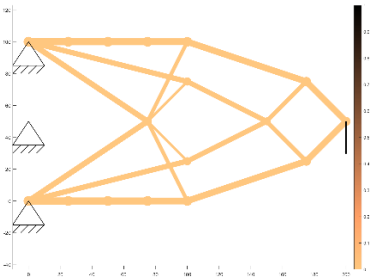
Figure 4.3(a): 9x5 mesh ground structure, cantilever	*Figure 4.3(b): Final structure with weight constraint, cantilever* **Compliance: 9.26**	*Figure 4.3(c): Final structure with GWP constraint, cantilever* **Compliance: 51.0**
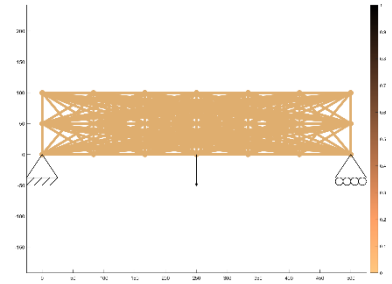	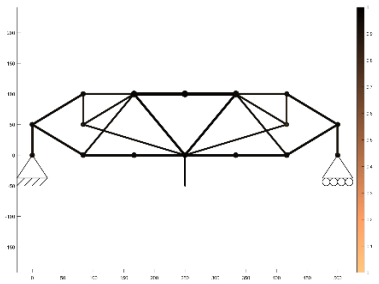	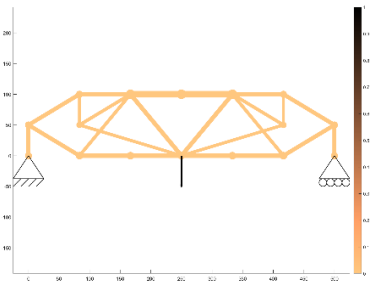
Figure 4.4(a): 7x3 mesh ground structure, simple beam	*Figure 4.4(b): Final structure with weight constraint, simple beam* **Compliance: 22.1**	*Figure 4.4(c): Final structure with GWP constraint, simple beam* **Compliance: 121.9**

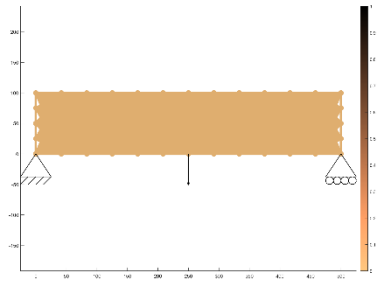	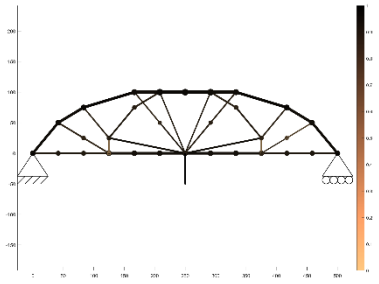	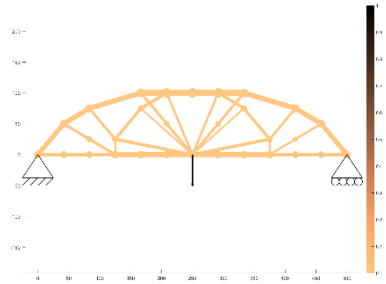
Figure 4.5(a): *13x5 mesh ground structure, simple beam*	*Figure 4.5(b):* *Final structure with weight constraint, simple beam* ***Compliance: 21.4***	*Figure 4.5(c):* *Final structure with GWP constraint, simple beam* ***Compliance: 116.0***

Colorbar: 0 = Timber, 1 = Steel

Table 4.3: Ground structures and optimized solutions for minimum compliance problems (4.1a) & (4.1b), 3D

Ground Structure	**(4.1a) Weight Constraint**	**(4.1b) GWP Constraint**
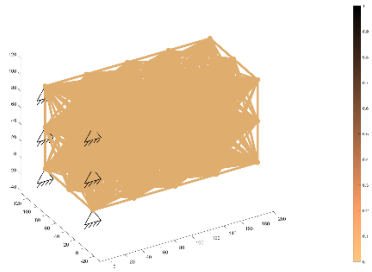	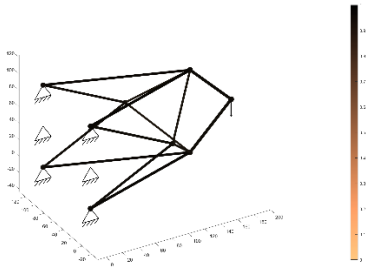	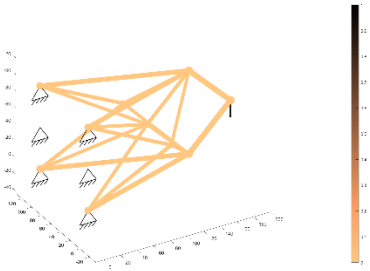
Figure 4.6(a): *5x3x3 mesh ground structure, cantilever*	*Figure 4.6(b):* *Final structure with weight constraint, cantilever* ***Compliance: 12.4***	*Figure 4.6(c):* *Final structure with GWP constraint, cantilever* ***Compliance: 66.3***
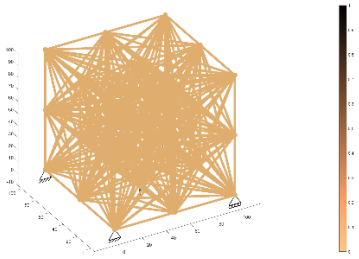	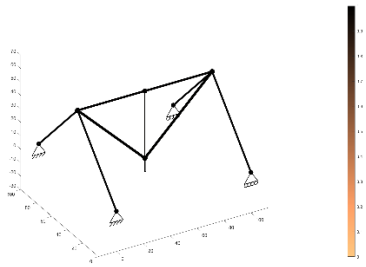	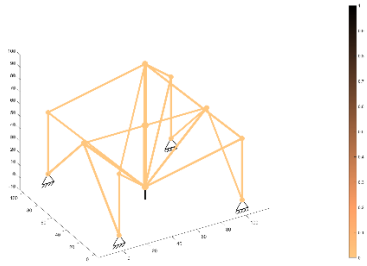
Figure 4.7(a): *3x3x3 mesh ground structure, vault*	*Figure 4.7(b):* *Final structure with weight constraint, vault* ***Compliance: 17.9***	*Figure 4.7(c):* *Final structure with GWP constraint, vault* ***Compliance: 98.9***

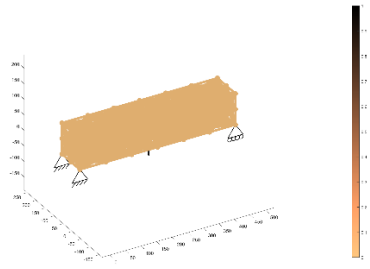

Figure 4.8(a):
7x3x3 mesh ground structure, simple beam

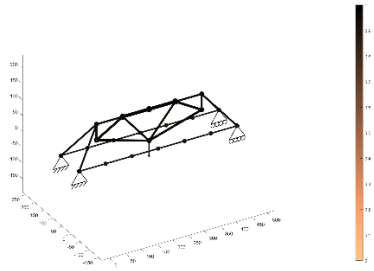

Figure 4.8(b):
Final structure with weight constraint, simple beam
Compliance: 24.1

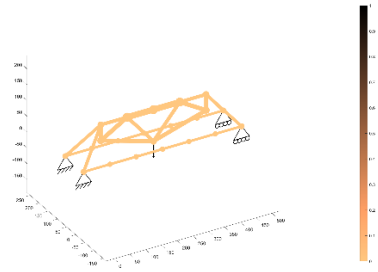

Figure 4.8(c):
Final structure with GWP constraint, simple beam
Compliance: 130.7

Colorbar: 0 = Timber, 1 = Steel

For each structure subject to a weight constraint (middle columns of Tables 4.2 & 4.3), the final solution was an all-steel truss. This makes sense because per unit volume, steel is 18 times stiffer than timber, but only 14 times heavier. In other words, steel is 1.3 times stiffer per unit weight than timber. Steel is therefore the preferred material in a maximum stiffness (min compliance) problem subject to a weight constraint.

On the other hand, when each of these structures were subject to a GWP constraint (right columns of Tables 4.2 & 4.3), the final solution was an all-timber truss. This also makes sense because per unit volume, steel is 18 times stiffer than timber, but 47 times more polluting. In other words, timber is 2.6 times stiffer per unit mass of embodied carbon compared to steel. Timber is therefore the preferred material in a maximum stiffness problem subject to a GWP constraint.

The fact that the solution produced by the optimizer agrees with our intuition suggests that the MATLAB script and the fmincon optimizer is working as intended, across a variety of 2D and 3D meshes and structures. Note that for the 3D vault (Figures 4.7(b)(c)), the timber structure is more redundant than its steel counterpart. This is not caused by timber elements hitting the upper bound A_{max}. Possible reasons behind the timber structure being more redundant include (i) timber is less stiff, and (ii) the 3D vault problem might be less stable than other structures; further investigation is needed to fully understand this phenomenon, which is out of the scope of this project.

5. Multi-Material Truss: Stress-Constrained Problem

5.1 Problem Formulation

Since a minimum compliance problem in (4.1a) and (4.1b) only takes the stiffness but not the strength of each material into account, an alternative problem formulation that takes material strength into account is needed to create trusses composed of multiple materials. A minimum GWP problem in (5.1a) and (5.1b) subject to stress constraints satisfies this requirement.

The first problem formulation (5.1a) uses real material stress constraints, while the second formulation (5.1b) models steel as a tension-only material and timber as a compression-only material. These two formulations are defined to explore the differences between (i) allowing the optimizer freedom to choose which material to use in tension or compression, and (ii) enforcing the optimizer to choose only timber for compression and steel for tension. For instance, in real-world design, formulation (5.1b) would be useful for avoiding the limit state of compression buckling in steel. (Note that buckling is not considered in this study.)

(Eq. 5.1a) – Minimum GWP subject to real stress constraints

$$
\begin{aligned}
&\underset{A^e,\,x^e}{minimize} && \textstyle\sum_{e\in\Omega} A^e L^e \rho^e ECC^e && \leftarrow \text{GWP}\\
&subject\ to && K(A,x)u = F && \leftarrow \text{Static Equilibrium}\\
& && \sigma_{min} \le \sigma^e \le \sigma_{max} \quad \forall\ e \in \Omega && \leftarrow \text{Stress Constraints}\\
& && A_{min} \le A^e \le A_{max} \quad \forall\ e \in \Omega && \leftarrow \text{Bounds on } A^e\\
& && 0 \le x^e \le 1 \quad \forall\ e \in \Omega && \leftarrow \text{Bounds on } x^e
\end{aligned}
$$

where:

$$E^e = x^e \Delta E + E_{timber}\,, \qquad \Delta E = E_{steel} - E_{timber} \qquad \text{(Eq. 5.2)}$$

$$\rho^e ECC^e = x^e \Delta(\rho ECC) + \rho_{timber} ECC_{timber}\,,$$

$$\Delta(\rho ECC) = \rho_{steel} ECC_{steel} - \rho_{timber} ECC_{timber} \qquad \text{(Eq. 5.3)}$$

$$\sigma_{min,timber} = -1250\ psi\,, \qquad \sigma_{max,timber} = +950\ psi \qquad \text{(Eq. 5.4)}$$

$$\sigma_{min,steel} = -50000\ psi\,, \qquad \sigma_{max,steel} = +50000\ psi \qquad \text{(Eq. 5.5)}$$

$$\sigma_{min} = (x^e)^{\eta}(\sigma_{min,steel} - \sigma_{min,timber}) + \sigma_{min,timber} \qquad \text{(Eq. 5.6)}$$

$$\sigma_{max} = (x^e)^{\eta}(\sigma_{max,steel} - \sigma_{max,timber}) + \sigma_{max,timber} \qquad \text{(Eq. 5.7)}$$

(Eq. 5.1b) – Minimum GWP subject to modified stress constraints

$$
\begin{aligned}
&\underset{A^e,\,x^e}{minimize} && \textstyle\sum_{e\in\Omega} A^e L^e \rho^e ECC^e && \leftarrow \text{GWP}\\
&subject\ to && K(x)u = F && \leftarrow \text{Static Equilibrium}\\
& && \sigma_{min} \le \sigma^e \le \sigma_{max} \quad \forall\ e \in \Omega && \leftarrow \text{Stress Constraints}\\
& && A_{min} \le A^e \le A_{max} \quad \forall\ e \in \Omega && \leftarrow \text{Bounds on } A^e\\
& && 0 \le x^e \le 1 \quad \forall\ e \in \Omega && \leftarrow \text{Bounds on } x^e
\end{aligned}
$$

where:

E^e and $\rho^e ECC^e$ are as defined in Eqs. 5.2 & 5.3,

but the stress limits are modified to Eqs. 5.8 & 5.9:

$\sigma_{min,timber} = -1250\ psi$, $\sigma_{max,timber} = +0\ psi$ (Eq. 5.8)

$\sigma_{min,steel} = -0\ psi$, $\sigma_{max,steel} = +50000\ psi$ (Eq. 5.9)

σ_{min} and σ_{max} remain as defined in Eqs. 5.6 & 5.7.

Notice that, for a stress-constrained problem, SIMP interpolation is no longer used for E^e and ρ^e. Instead, E^e and ρ^e (or $\rho^e ECC^e$ in the context of min GWP) are interpolated linearly from x^e. Instead of penalizing the intermediate stiffnesses and densities, the intermediate stress constraints are penalized (Eqs. 5.6 & 5.7) to encourage the optimizer to converge to either timber (x^e = 0) or steel (x^e = 1) for all elements. For this study, SIMP interpolation is used with η = 3 in the stress constraints.

5.2 Sensitivity Analysis

The sensitivities for the stress constraints can be derived using direct differentiation. Here, we derive the sensitivities with respect to design variables A^e and x^e:

For a hypothetical design problem with n = 2 truss elements, the constraint function is:

$$
g = \begin{vmatrix} \sigma_{min,1} - \sigma_1 \\ \sigma_{min,2} - \sigma_2 \\ \sigma_1 - \sigma_{max,1} \\ \sigma_2 - \sigma_{max,2} \end{vmatrix} = \begin{vmatrix} (x^1)^\eta(\sigma_{min,steel} - \sigma_{min,timber}) + \sigma_{min,timber} - \sigma_1 \\ (x^2)^\eta(\sigma_{min,steel} - \sigma_{min,timber}) + \sigma_{min,timber} - \sigma_2 \\ \sigma_1 - [(x^1)^\eta(\sigma_{max,steel} - \sigma_{max,timber}) + \sigma_{max,timber}] \\ \sigma_2 - [(x^2)^\eta(\sigma_{max,steel} - \sigma_{max,timber}) + \sigma_{max,timber}] \end{vmatrix} \quad \text{(Eq. 5.10)}
$$

The stress for each element is:

$$
\sigma_e = \frac{Axial\ Load}{A_e} = \frac{T_e K_e d_e}{A_e} = \frac{E_e A_e T_e K_{e,0} d_e}{A_e} = E_e T_e K_{e,0} d_e \quad \text{(Eq. 5.11)}
$$

where T_e, K_e, and d_e are the element transformation matrix, element stiffness matrix, and element displacement vector, respectively [37].

The derivative of the stress function with respect to A_j is:

$$\frac{\partial \sigma_e}{\partial A_j} = E_e T_e K_{e,0} \frac{\partial d_e}{\partial A_j} \qquad \text{(Eq. 5.12)}$$

By direct differentiation on the equilibrium constraint, the derivative of d_e with respect to A_j can be extracted from the derivative of d with respect to A_j:

$$Kd - F = 0 \qquad \text{(Eq. 5.13)}$$

$$\frac{\partial K}{\partial A_j} d + K \frac{\partial d}{\partial A_j} = 0 \qquad \text{(Eq. 5.14)}$$

$$\frac{\partial d}{\partial A_j} = -K^{-1}\left(\frac{\partial K}{\partial A_j} d\right) \qquad \text{(Eq. 5.15)}$$

$$\frac{\partial d_e}{\partial A_j} = get\_de\_from\_d\left(\frac{\partial d}{\partial A_j}\right) \qquad \text{(Eq. 5.16)}$$

Hence, the sensitivities of the constraint g with respect to A_j are:

$$\frac{\partial g_e}{\partial A_j} = -E_e T_e K_{e,0} \frac{\partial d_e}{\partial A_j} \qquad \text{(Eq. 5.17)}$$

$$\frac{\partial g_{e+n}}{\partial A_j} = E_e T_e K_{e,0} \frac{\partial d_e}{\partial A_j} \qquad \text{(Eq. 5.18)}$$

Now, for the derivative of stress (Eq. 5.11) with respect to E_j:

$$\frac{\partial \sigma_e}{\partial E_j} = T_e K_{e,0} d_e + E_e T_e K_{e,0} \frac{\partial d_e}{\partial E_j} \qquad \text{if } e = j \qquad \text{(Eq. 5.19)}$$

$$\frac{\partial \sigma_e}{\partial E_j} = E_e T_e K_{e,0} \frac{\partial d_e}{\partial E_j} \qquad \text{if } e \neq j \qquad \text{(Eq. 5.20)}$$

Where $\frac{\partial d_e}{\partial E_j}$ is derived similar to Eq. 5.13 – Eq. 5.16:

$$\frac{\partial d}{\partial E_j} = -K^{-1}\left(\frac{\partial K}{\partial E_j} d\right) \qquad \text{(Eq. 5.21)}$$

$$\frac{\partial d_e}{\partial E_j} = get\_de\_from\_d\left(\frac{\partial d}{\partial E_j}\right) \qquad \text{(Eq. 5.22)}$$

To convert $\frac{\partial \sigma_e}{\partial E_j}$ to $\frac{\partial \sigma_e}{\partial x_j}$:

$$\frac{\partial \sigma_e}{\partial x_j} = \frac{\partial \sigma_e}{\partial E_j} \frac{\partial E_j}{\partial x_j} = \frac{\partial \sigma_e}{\partial E_j} (\Delta E) \qquad \text{(Eq. 5.23)}$$

The derivatives of $\sigma_{min,e}$ and $\sigma_{max,e}$ with respect to x_j (only when $e = j$; zero if $e \neq j$) are:

$$\frac{\partial \sigma_{min,e}}{\partial x_e} = \eta(x_e)^{\eta-1}(\sigma_{min,steel} - \sigma_{min,timber}) \qquad \text{(Eq. 5.24)}$$

$$\frac{\partial \sigma_{max,e}}{\partial x_e} = \eta(x_e)^{\eta-1}(\sigma_{max,steel} - \sigma_{max,timber}) \qquad \text{(Eq. 5.25)}$$

Hence, the sensitivities of the constraint g with respect to x_j are:

$$\frac{\partial g_e}{\partial x_j} = \frac{\partial \sigma_{min,e}}{\partial x_e} - \frac{\partial \sigma_e}{\partial x_j} \qquad \text{(Eq. 5.26)}$$

$$\frac{\partial g_{e+n}}{\partial x_j} = \frac{\partial \sigma_e}{\partial x_j} - \frac{\partial \sigma_{max,e}}{\partial x_e} \qquad \text{(Eq. 5.27)}$$

5.3 Results & Discussion

Cantilevers (Figures 5.1 & 5.2), a simple beam (Figure 5.3), and a vault (Figure 5.4) of different mesh densities in 2D and 3D were topology optimized subject to stress constraints, with a minimum GWP objective. Starting with fully connected ground structures, fmincon with the interior-point algorithm was called to perform the optimization. Initial conditions were $A_0 = 5$ in^2 and $x_0 = 0.5$ (hypothetical intermediate material), with A^e bound between 1e-3 and 15, and x^e bound between 0 and 1.

The dimensions of each studied structure are shown in Table 5.1. For all structures except the 3D vault, the magnitude of the applied load is 10,000 lb. For the 3D vault, the applied load is 20,000 lb.

Table 5.1: Dimensions of each structure

Structure	Height (in)	Length (in)	Depth (in)
2D cantilever (Figs. 5.1 & 5.2)	100	200	N/A
2D simple beam (Fig. 5.3)	100	500	N/A
3D vault (Fig. 5.4)	100	100	100

Ground structures are shown in the left columns of Tables 5.2 & 5.3. Optimized solutions using real stress constraints (problem formulation 5.1a) are shown in the middle columns of Tables 5.2 & 5.3, and optimized solutions using modified stress constraints (problem formulation 5.1b) are shown in the right columns. In general, the real stress limit formulation yielded all-steel trusses (with one exception), and the modified stress limit formulation yielded steel-timber trusses.

Note that while the sensitivities derived in Section 5.2 (using direct differentiation) gave excellent solutions for 2D trusses, its solutions for 3D structures sometimes included an odd, unhelpful “floating” element. Therefore, finite difference sensitivities were used for the 3D vault shown in Figure 5.4, which eliminated the “floating” elements. It is not immediately apparent why direct differentiation sensitivities works well for 2D trusses but not 3D trusses; further investigation is needed to fully understand this phenomenon, which is out of the scope of this project.

Table 5.2: Ground structures and optimized solutions

for multi-material stress constrained problems (5.1a) and (5.1b), 2D

Ground Structure	**(5.1a) Min GWP with Real Stress Constraints**	**(5.1b) Min GWP with Modified Stress Constraints**
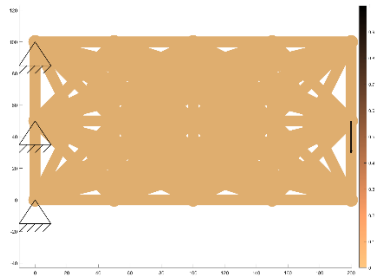 *Figure 5.1(a):* *5x3 mesh ground structure, cantilever*	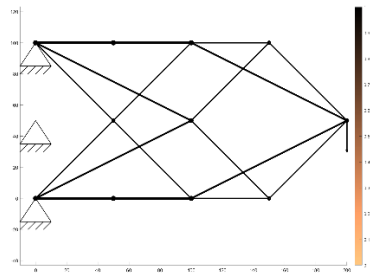 *Figure 5.1(b):* *Final structure with real stress constraint, cantilever* ***Objective = 62.9***	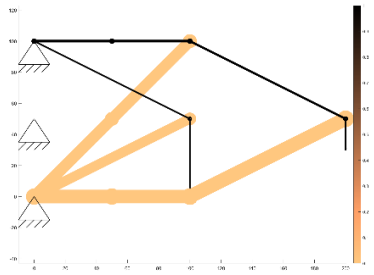 *Figure 5.1(c):* *Final structure with modified stress constraint, cantilever* ***Objective = 57.5***
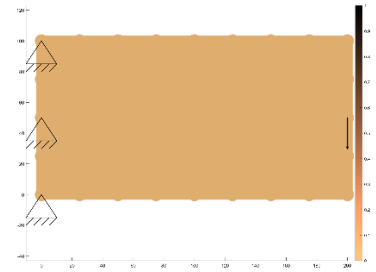 *Figure 5.2(a):* *9x5 mesh, cantilever*	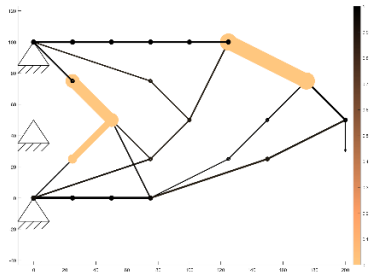 *Figure 5.2(b):* *Final structure with real stress constraint, cantilever* ***Objective = 70.7***	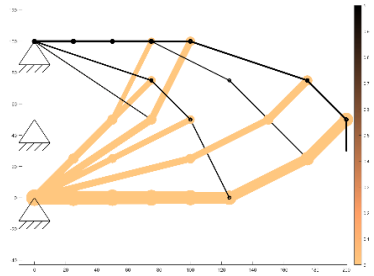 *Figure 5.2(c):* *Final structure with modified stress constraint, cantilever* ***Objective = 60.6***
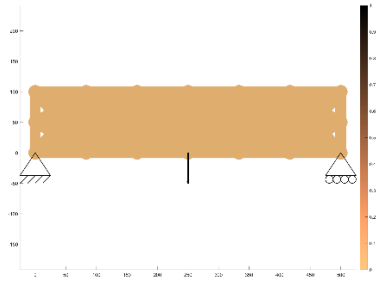 *Figure 5.3(a):* *7x3 mesh, simple beam*	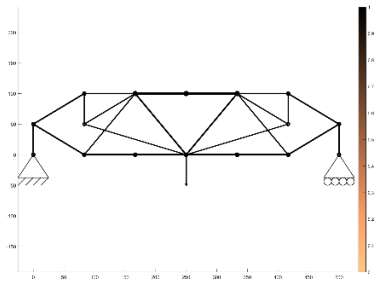 *Figure 5.3(b):* *Final structure with real stress constraint, simple beam* ***Objective = 99.9***	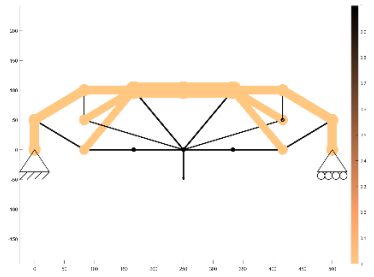 *Figure 5.3(c):* *Final structure with modified stress constraint, simple beam* ***Objective = 90.2***

Colorbar: 0 = Timber, 1 = Steel

Table 5.3: Ground structures and optimized solutions
for multi-material stress constrained problems (5.1a) and (5.1b), 3D

Ground Structure	**(5.1a) Min GWP with Real Stress Constraints**	**(5.1b) Min GWP with Modified Stress Constraints**
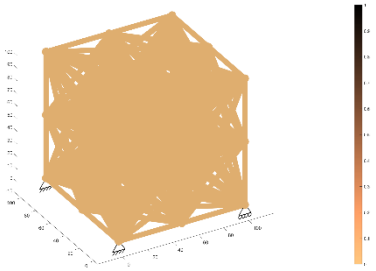 *Figure 5.4(a): 3x3x3 mesh, vault*	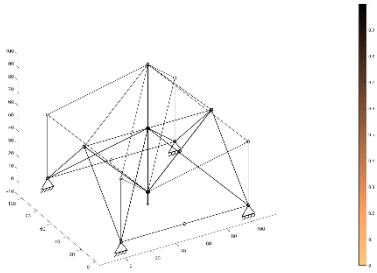 *Figure 5.4(b): Final structure with real stress constraint, vault* ***Objective = 44.8***	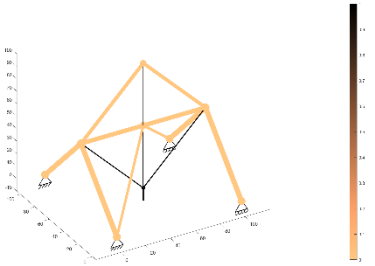 *Figure 5.4(c): Final structure with modified stress constraint, vault* ***Objective = 39.4***

Colorbar: 0 = Timber, 1 = Steel

In each of the four studied structures, the solution obtained using real stress constraints ("real stress solution") was less optimal than the one obtained using modified stress constraints ("modified stress solution"). For the 5x3 cantilever, the real stress solution (Figure 5.1(b)) was 9.4% more polluting than the modified stress solution (Figure 5.1(c)). Similarly, the real stress solutions of the 9x5 cantilever (Figure 5.2(b)), 7x3 simple beam (Figure 5.3(b)), and the 3x3x3 vault (Figure 5.4(b)) were 16.7%, 10.8%, and 13.7% more polluting than their respective modified stress counterparts (Figures 5.2(c), 5.3(c) & 5.4(c)).

Examining the middle columns of Tables 5.2 & 5.3, the real stress solutions favored all-steel trusses, except for the 9x5 cantilever, where 3 timber members were used (2 in tension and 1 in compression). This is in contrast with the right columns of Tables 5.2 & 5.3, where both steel and timber members were employed in the trusses, with steel carrying tensile loads and timber resisting compressive loads. From an embodied carbon perspective, this arrangement of steel and timber members is ideal since timber is stronger in compression per unit CO_2 and steel is stronger in tension per unit CO_2 (see Table 2.1). This is evidenced by the lower GWP objectives of the modified stress solutions compared to those of the real stress solutions.

Again, we observe two different topologies for the 3x3x3 vault solution (Figures 5.4(b)(c)), like its min compliance counterparts in Section 4.3. Here, the real stress solution, featuring an all-steel truss, appears to be more redundant. The variety of optimized topologies observed for the 3x3x3 vault suggests that many

solutions (local minima) may be more or less equally viable, perhaps owing to its square, symmetric design domain.

It is somewhat surprising that the global optimum for each structure could not achieved with real stress limits. This phenomenon is most likely due to the non-linearity of the stress-constrained problem, which is further explored in Section 5.4. This non-linearity also manifests itself in producing asymmetric solutions (Figures 5.1(c) & 5.2(b)(c)).

5.4 Objective Landscape

In order to understand why the best optimized design for minimizing global warming potential can only by using modified stress constraints (Eq. 5.1b), a simplified truss topology optimization problem of a single bar subject to an axial load is studied.

Table 5.4: Ground and optimized structures using real or modified stress limits for a single-bar problem

Ground Structure	**Optimized Structure Using Real Stress Constraints (5.1a)**	**Optimized Structure Using Modified Stress Constraints (5.1b)**
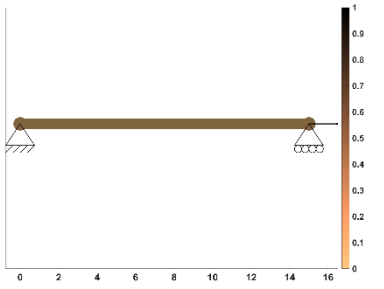	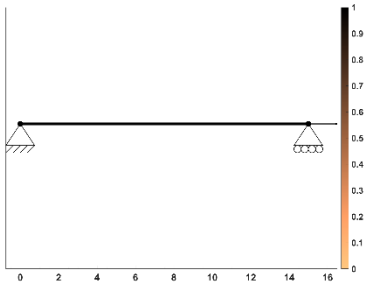	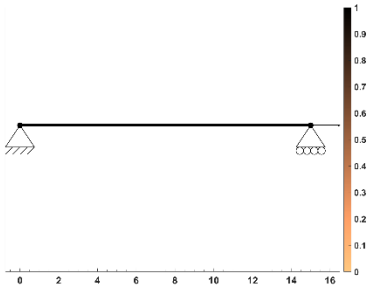
Figure 5.6(a): Single bar in tension	*Figure 5.6(b): Steel bar in tension* ***Objective = 1.87***	*Figure 5.6(c): Steel bar in tension* ***Objective = 1.87***
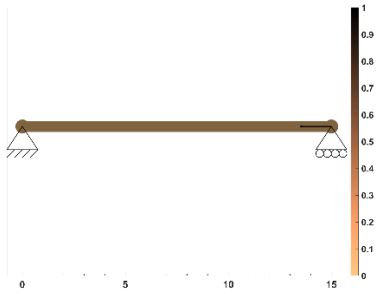	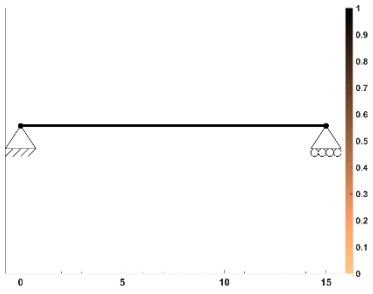	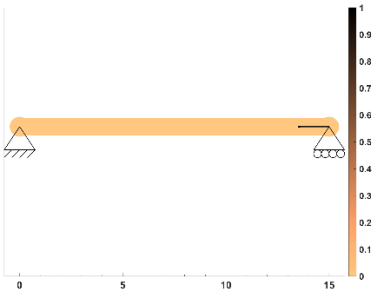
Figure 5.7(a): Single bar in compression	*Figure 5.7(b): Steel bar in compression* ***Objective = 1.87***	*Figure 5.7(c): Timber bar in compression* ***Objective = 1.56***

A_0 = 5; A_{min} = 1e-3; A_{max} = 15; Colorbar: 0 = Timber, 1 = Steel

As shown in Table 5.4, a single bar subjected to either a tensile load (Figure 5.6(a)) or a compressive load (Figure 5.7(a)) of magnitude P = 15 kips is topology optimized, starting with a ground structure of A_0 = 5 in^2 and x_0 = 0.5 (hypothetical material in between timber and steel). The length of the member was 15 in. The obtained solutions with real stress constraints are shown in Figures 5.6(b) & 5.7(b). In Figures 5.6(c) & 5.7(c) shows the results obtained when the stress constraints are modified so that $\sigma_{max,timber} = +0$, $\sigma_{min,steel} = -0$.

Under real stress constraints (Eq. 5.1a), the tensile bar converges to a steel bar in Figure 5.6(b), as expected, since steel is stronger in tension per unit embodied carbon. However, the compressed bar also converges to a steel bar in Figure 5.7(b), which is unexpected since timber is stronger in compression per unit embodied carbon (see discussion in Section 5.3). Modified stress constraints (Eq. 5.1b) are needed to guide the optimizer to choose timber for a compressed bar, as shown in Figure 5.7(c). The global warming potential for the timber bar in compression is f = 1.56, which is lower than that of the steel bar in compression (f = 1.87). A timber bar is hence the most optimal solution for compression.

To investigate why modified stress constraints are necessary to reach the global minimum, the objective landscape for the single bar is plotted using graphical optimization (in Table 5.5) and studied.

Table 5.5: Objective landscapes for a single-bar problem with real or modified stress constraints

	Real Stress Constraints (5.1a)	**Modified Stress Constraints (5.1b)**
Tension	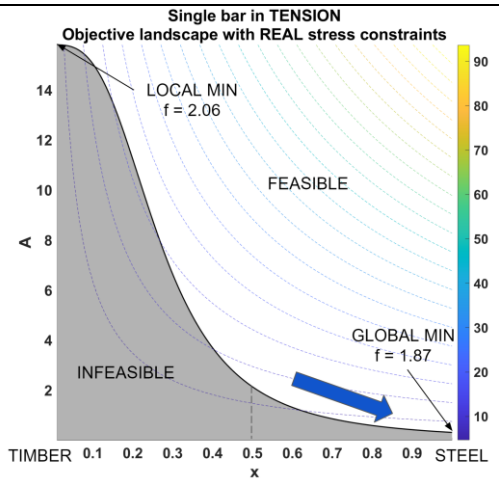 *Figure 5.8(a): Objective landscape for a tensile bar with real stress constraints*	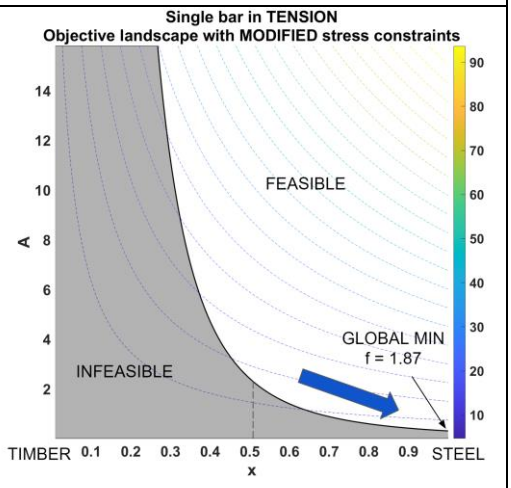 *Figure 5.8(b): Objective landscape for a tensile bar with modified stress constraints*
Compression	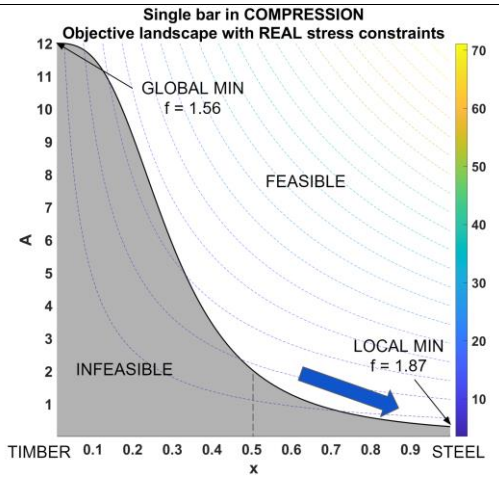 *Figure 5.9(a): Objective landscape for a compressed bar with real stress constraints*	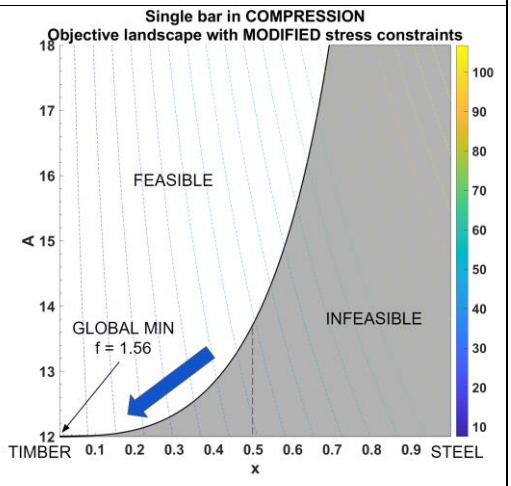 *Figure 5.9(b): Objective landscape for a compressed bar with modified stress constraints*

*Colorbars and contour lines represent objective values

Using information about the optimized structures in Table 5.4, the direction of convergence is indicated with blue arrows on Figures 5.8 & 5.9. In Figure 5.8(a), for a single bar in tension, the problem correctly converges to the global minimum (steel) under real stress constraints. In Figure 5.8(b), modifying the stress constraints (such that timber takes no load in tension) removes the local minimum at x = 0 (timber), which does not affect the direction of convergence, since the optimizer was already choosing the optimal material (steel) correctly.

In Figure 5.9(a), for a single bar in compression, the problem converges to a local minimum (steel) under real stress constraints, instead of the global minimum (timber). Studying the objective landscape, we conclude that this is most likely due to nonlinearities in the problem, in both the stress-constraint function (the curve dividing the feasible and infeasible regions) and the objective function (the contour lines). Nonlinearity in the stress-constraint function is caused by the SIMP power factor η, and nonlinearity in the objective function is caused by multiplying multiple design variables (A^e and x^e) together. Increasing nonlinearities causes the optimization problem to become harder to solve, which increases the likelihood that a local minimum, instead of a global minimum, is reached.

As shown in Figure 5.9(b), the problem of being "stuck" in a local minimum is resolved by eliminating the local minimum itself. Modifying the stress constraints (such that steel takes no load in tension) removes the local minimum at $x = 1$ (steel), encouraging the optimizer to converge to the only minimum remaining, at $x = 0$ (timber).

6. Conclusions

In the first part of this project, min compliance problems subject to either a structural weight constraint or global warming potential (GWP) constraint are studied for multi-material trusses. We find that the weight-constrained problems produced all-steel truss solutions, while GWP-constrained problems produced all-timber truss solutions. These results agree with our initial expectations, since steel is stiffer per unit weight and timber is stiffer per unit CO_2. While these results may seem trivial, it verified that our MATLAB code is working as intended. Moreover, these results highlight that, in the context of multi-material structures, the weight-constrained solution may be different than the GWP-constrained solution. This contrasts with single-material structures, where the weight-constrained solution is always equal to the GWP-constrained solution.

To take material strength into account, the stress-constrained problem with a minimum GWP objective is investigated. Two problem formulations are studied and compared: one with real material stress constraints; and one with modified stress constraints, where timber was considered as a compression-only material and steel as a tension-only material. Across all studied structures, the real stress solutions are more polluting than the modified stress solutions by 9.4% – 16.7%. This is because the real stress solutions tended to favor steel over timber, regardless of whether the truss element was in tension or compression. The designs produced by real stress constraints are somewhat surprising to us; since steel is stronger in tension (per unit CO_2) and timber is stronger in compression (per unit CO_2), we expected both materials to be utilized in their respective strengths. On the other hand, the modified stress solutions chose timber for compressive struts and steel for tensile bars, resulting in the lower GWP designs as expected.

To investigate why the real stress formulation could not achieve the better, "greener" designs, the objective landscape of a single bar in either tension or compression is studied. We find that, due to non-linearities in the stress-constrained problem and the SIMP interpolation, the real stress objective landscape favored a convergence towards the steel minimum in both compressive and tensile cases. While the steel minimum is the global minimum for the tensile case, the timber minimum is the global minimum for the compressive case. To encourage the optimizer to choose the global minimum every time, modified stress constraints are introduced, which eliminates the local minima. The modified stress-constrained formulation successfully produced hybrid trusses with timber and steel placed in their most efficient arrangements for embodied carbon objectives.

The field of topology optimization for structural design and embodied carbon objectives remains largely unexplored. Possible future works related to this thesis include (i) incorporating buckling stress into the

stress-constrained problem, (ii) performing a similar simulation with other pairs of materials, (iii) extending truss topology optimization to frame topology optimization, (iv) investigating the reasons behind the instability of the 3D vault problem, and (v) exploring why the direct differentiation sensitivities work well for 2D trusses but not 3D trusses.

7. References

[1] C. De Wolf, "Low carbon pathways for structural design : embodied life cycle impacts of building structures," Thesis, Massachusetts Institute of Technology, 2017.

[2] "Use of energy in explained - U.S. Energy Information Administration (EIA)." https://www.eia.gov/energyexplained/use-of-energy/ (accessed May 06, 2020).

[3] C. R. Iddon and S. K. Firth, "Embodied and operational energy for new-build housing: A case study of construction methods in the UK," *Energy Build.*, vol. 67, pp. 479–488, Dec. 2013, doi: 10.1016/j.enbuild.2013.08.041.

[4] Z. Luo, L. Yang, and J. Liu, "Embodied carbon emissions of office building: A case study of China's 78 office buildings," *Build. Environ.*, vol. 95, pp. 365–371, Jan. 2016, doi: 10.1016/j.buildenv.2015.09.018.

[5] C. De Wolf, F. Pomponi, and A. Moncaster, "Measuring embodied carbon dioxide equivalent of buildings: A review and critique of current industry practice," *Energy Build.*, vol. 140, pp. 68–80, Apr. 2017, doi: 10.1016/j.enbuild.2017.01.075.

[6] A. M. Moncaster and K. E. Symons, "A method and tool for 'cradle to grave' embodied carbon and energy impacts of UK buildings in compliance with the new TC350 standards," *Energy Build.*, vol. 66, pp. 514–523, Nov. 2013, doi: 10.1016/j.enbuild.2013.07.046.

[7] R. J. Cole and P. C. Kernan, "Life-cycle energy use in office buildings," *Build. Environ.*, vol. 31, no. 4, pp. 307–317, Jul. 1996, doi: 10.1016/0360-1323(96)00017-0.

[8] P. Chastas, T. Theodosiou, K. J. Kontoleon, and D. Bikas, "Normalising and assessing carbon emissions in the building sector: A review on the embodied CO2 emissions of residential buildings," *Build. Environ.*, vol. 130, pp. 212–226, Feb. 2018, doi: 10.1016/j.buildenv.2017.12.032.

[9] F. Pomponi and A. Moncaster, "Embodied carbon mitigation and reduction in the built environment – What does the evidence say?," *J. Environ. Manage.*, vol. 181, pp. 687–700, Oct. 2016, doi: 10.1016/j.jenvman.2016.08.036.

[10] T. Häkkinen, M. Kuittinen, A. Ruuska, and N. Jung, "Reducing embodied carbon during the design process of buildings," *J. Build. Eng.*, vol. 4, pp. 1–13, Dec. 2015, doi: 10.1016/j.jobe.2015.06.005.

[11] B. G. Stern, "Minimizing embodied carbon in multi-material structural optimization of planar trusses," Thesis, Massachusetts Institute of Technology, 2018.

[12] M. P. Bendsøe and O. Sigmund, *Topology Optimization: Theory, Methods, and Applications*. Springer Science & Business Media, 2004.

[13] L. L. Stromberg, A. Beghini, W. F. Baker, and G. H. Paulino, "Application of layout and topology optimization using pattern gradation for the conceptual design of buildings," *Struct. Multidiscip. Optim.*, vol. 43, no. 2, pp. 165–180, Feb. 2011, doi: 10.1007/s00158-010-0563-1.

[14] *National Design Specification (NDS) Supplement: Design Values for Wood Construction*, 2018 Edition. American Wood Council.

[15] G. Hammond, C. Jones, F. Lowrie, P. Tse, Building Services Research and Information Association, and University of Bath, *Embodied carbon: the Inventory of Carbon and Energy (ICE)*. Bracknell: BSRIA, 2011.

[16] "AD Classics: Scottish Parliament Building / Enric Miralles," *ArchDaily*, Feb. 14, 2011. http://www.archdaily.com/111869/ad-classics-the-scottish-parliament-enric-miralles (accessed May 06, 2020).

[17] "University of Massachusetts Amherst Design Building / Leers Weinzapfel Associates," *ArchDaily*, May 25, 2017. http://www.archdaily.com/872034/university-of-massachusetts-amherst-design-building-leers-weinzapfel-associates (accessed May 06, 2020).

[18] *Steel Construction Manual*, 15th ed. American Institute of Steel Construction, 2017.

[19] M. P. Bendsøe and O. Sigmund, "Material interpolation schemes in topology optimization," *Arch. Appl. Mech.*, vol. 69, no. 9, pp. 635–654, Nov. 1999, doi: 10.1007/s004190050248.

[20] A. T. Gaynor, N. A. Meisel, C. B. Williams, and J. K. Guest, "Multiple-Material Topology Optimization of Compliant Mechanisms Created Via PolyJet Three-Dimensional Printing," *J. Manuf. Sci. Eng.*, vol. 136, no. 6, Dec. 2014, doi: 10.1115/1.4028439.
[21] L. Yin and G. K. Ananthasuresh, "Topology optimization of compliant mechanisms with multiple materials using a peak function material interpolation scheme," *Struct. Multidiscip. Optim.*, vol. 23, no. 1, pp. 49–62, Dec. 2001, doi: 10.1007/s00158-001-0165-z.
[22] S. Watts and D. A. Tortorelli, "An n-material thresholding method for improving integerness of solutions in topology optimization," *Int. J. Numer. Methods Eng.*, vol. 108, no. 12, pp. 1498–1524, 2016, doi: 10.1002/nme.5265.
[23] G. Cheng, "Some aspects of truss topology optimization," *Struct. Optim.*, vol. 10, no. 3, pp. 173–179, Dec. 1995, doi: 10.1007/BF01742589.
[24] G. I. N. Rozvany, "Difficulties in truss topology optimization with stress, local buckling and system stability constraints," *Struct. Optim.*, vol. 11, no. 3, pp. 213–217, Jun. 1996, doi: 10.1007/BF01197036.
[25] M. Zhou, "Difficulties in truss topology optimization with stress and local buckling constraints," *Struct. Optim.*, vol. 11, no. 2, pp. 134–136, Apr. 1996, doi: 10.1007/BF01376857.
[26] X. Guo, G. Cheng, and K. Yamazaki, "A new approach for the solution of singular optima in truss topology optimization with stress and local buckling constraints," *Struct. Multidiscip. Optim.*, vol. 22, no. 5, pp. 364–373, Dec. 2001, doi: 10.1007/s00158-001-0156-0.
[27] A. G. Weldeyesus, J. Gondzio, L. He, M. Gilbert, P. Shepherd, and A. Tyas, "Adaptive solution of truss layout optimization problems with global stability constraints," *Struct. Multidiscip. Optim.*, vol. 60, no. 5, pp. 2093–2111, Nov. 2019, doi: 10.1007/s00158-019-02312-9.
[28] P. N. Poulsen, J. F. Olesen, and M. Baandrup, "Truss optimization applying finite element limit analysis including global and local stability," *Struct. Multidiscip. Optim.*, Mar. 2020, doi: 10.1007/s00158-019-02468-4.
[29] P. Kumar, "Optimal force transmission in reinforced concrete deep beams," *Comput. Struct.*, vol. 8, no. 2, pp. 223–229, Apr. 1978, doi: 10.1016/0045-7949(78)90026-3.
[30] M. A. Ali and R. N. White, "Automatic generation of truss model for optimal design of reinforced concrete structures," *ACI Struct. J.*, vol. 98, no. 4, pp. 431–442, 2001.
[31] A. Asadpoure, M. Tootkaboni, and J. K. Guest, "Robust topology optimization of structures with uncertainties in stiffness – Application to truss structures," *Comput. Struct.*, vol. 89, no. 11, pp. 1131–1141, Jun. 2011, doi: 10.1016/j.compstruc.2010.11.004.
[32] M. Jalalpour, T. Igusa, and J. K. Guest, "Optimal design of trusses with geometric imperfections: Accounting for global instability," *Int. J. Solids Struct.*, vol. 48, no. 21, pp. 3011–3019, Oct. 2011, doi: 10.1016/j.ijsolstr.2011.06.020.
[33] A. Asadpoure, J. K. Guest, and L. Valdevit, "Incorporating fabrication cost into topology optimization of discrete structures and lattices," *Struct. Multidiscip. Optim.*, vol. 51, no. 2, pp. 385–396, Feb. 2015, doi: 10.1007/s00158-014-1133-8.
[34] W. Achtziger, "Truss topology optimization including bar properties different for tension and compression," *Struct. Optim.*, vol. 12, no. 1, pp. 63–74, Aug. 1996, doi: 10.1007/BF01270445.
[35] M. Stolpe and K. Svanberg, "A stress-constrained truss-topology and material-selection problem that can be solved by linear programming," *Struct. Multidiscip. Optim.*, vol. 27, no. 1, pp. 126–129, May 2004, doi: 10.1007/s00158-003-0364-x.
[36] S. Rakshit and G. K. Ananthasuresh, "Simultaneous material selection and geometry design of statically determinate trusses using continuous optimization," *Struct. Multidiscip. Optim.*, vol. 35, no. 1, pp. 55–68, Jan. 2008, doi: 10.1007/s00158-007-0116-4.
[37] Russell C. Hibbeler, *Structural Analysis*, 8th ed. Pearson Prentice Hall, 2012.
[38] P. W. Christensen and A. Klarbring, *An Introduction to Structural Optimization*. Springer Science & Business Media, 2008.
[39] M. P. Bendsøe, "Optimal shape design as a material distribution problem," *Struct. Optim.*, vol. 1, no. 4, pp. 193–202, Dec. 1989, doi: 10.1007/BF01650949.

[40] M. Zhou, Shyy Y. K., and H. L. Thomas, “Checkerboard and minimum member size control in topology optimization,” *Struct. Multidiscip. Optim.*, vol. 21, no. 2, pp. 152–158, Apr. 2001, doi: 10.1007/s001580050179.